[redacted] ~~CONFIDENTIAL~~

15959
16036

Copy
RM L

TECH LIBRARY KAFB, NM
0144720

NACA RM L58G29

7851

RESEARCH MEMORANDUM

ROCKET-MODEL INVESTIGATION TO DETERMINE THE LIFT AND PITCHING EFFECTIVENESS OF SMALL PULSE ROCKETS EXHAUSTED FROM THE FUSELAGE OVER THE SURFACE OF AN ADJACENT WING AT MACH NUMBERS FROM 0.9 TO 1.8

By C. William Martz

Langley Aeronautical Laboratory
Langley Field, Va.

[redacted]

[redacted] within the meaning of the [redacted] which in any [redacted]

NATIONAL ADVISORY COMMITTEE FOR AERONAUTICS

WASHINGTON
September 30, 1958

~~CONFIDENTIAL~~

[redacted]

Classification cancelled (or changed to UNCLASSIFIED)

By Authority of AHSA Tech Pub Announcement #39
(OFFICER AUTHORIZED TO CHANGE)

By 16 Feb 61
NAME AND

GRADE OF OFFICER MAKING CHANGE)

21 Mar 61
DATE

TECH LIBRARY KAFB, NM
0144720

NATIONAL ADVISORY COMMITTEE FOR AERONAUTICS

RESEARCH MEMORANDUM

ROCKET-MODEL INVESTIGATION TO DETERMINE THE LIFT AND PITCHING EFFECTIVENESS OF SMALL PULSE ROCKETS EXHAUSTED FROM THE FUSELAGE OVER THE SURFACE OF AN ADJACENT WING AT MACH NUMBERS FROM 0.9 TO 1.8*

By C. William Martz

SUMMARY

Experimental free-flight data have been obtained at Mach numbers from 0.9 to 1.8 on the normal force and pitching effectiveness of several small pulse rockets located in the fuselage of a rocket propelled model. The pulse rockets were arranged to exhaust in a spanwise direction over the surface of a tapered and unswept wing and thereby to induce a lifting load on the wing. Wing-damping data were obtained from the wing bending response to the pulse-rocket excitations, and longitudinal stability data were determined from the model response.

Results show that the normal forces induced by the pulse rockets were from 5 to 8 times as large as the corresponding thrust of the rockets. The peak angles of attack produced by the pulse-rocket disturbances were from 2 to 5 times as large as peak angles of attack calculated for vertically mounted pulse rockets at the same longitudinal stations (wing interference effects being neglected). This ratio was greater for the pulse rockets located nearer the wing leading edge.

INTRODUCTION

Previous investigations (for example, refs. 1 and 2) indicated that pulse rockets or jets exhausted in the proximity of aerodynamic surfaces induced considerable loads on these surfaces. This suggested that small rockets or air jets might be used as a means of flight control.

---

*Title, Unclassified.

AFMDC DAS 59-75-64

Also, their use in flutter testing to provide excitation of aerodynamic surfaces appeared desirable because their presence does not affect the response measurements.

A rocket model investigation was therefore conducted to measure the effectiveness of small pulse rockets both as lift and pitch control devices and as a means of exciting wing vibrations to obtain wing damping data. Mach numbers ranged from 1.8 to 0.9 and Reynolds number per foot varied from about 11×10^6 to 5×10^6.

Pulse-rocket-effectiveness data and wing-damping data (first bending mode) are presented. In addition, for the purpose of completeness, model longitudinal-stability data are presented with no analysis.

SYMBOLS

a_n model normal acceleration at center of gravity, g units

A amplitude of angle-of-attack oscillation envelope, deg

A_h amplitude of wing vibrometer oscillation envelope, g units

b exponential damping coefficient for model pitching mode, $-\frac{d(\log_e A)}{dt}$, per sec

b_h exponential damping coefficient for wing bending mode, $-\frac{d(\log_e A_h)}{dt}$, per sec

c wing chord, ft

$\bar{c}$ wing mean aerodynamic chord, 1.137 ft

C_m model pitching moment (about model center of gravity) coefficient based on $\bar{c}$

C_{m_α} $\frac{dC_m}{d\alpha}$, per deg; also $\frac{-I_Y\omega^2(1 + \xi^2)}{57.3qS\bar{c}}$

C_N model normal-force coefficient, $\frac{(\text{Model weight})(a_n)}{qS}$

$\lvert\Delta C_N\rvert$	maximum absolute value of incremental normal-force coefficient due to initial burning of pulse rockets
C_{N_α}	normal-force-curve slope, $\frac{dC_N}{d\alpha}$, per deg
d	pulse-rocket location along exposed wing root chord, in. from leading edge
g	acceleration of gravity, 32.2 ft/sec^2
I_Y	model moment of inertia in pitch, 7.12 slug-ft^2
k	wing reduced frequency, $\frac{\omega_h \bar{c}}{2V}$
M	Mach number
q	free-stream dynamic pressure, lb/sq ft
R	Reynolds number per foot
S	total wing area, 4.05 sq ft
t	time, sec
V	free-stream velocity, ft/sec
α	angle of attack at model center of gravity, deg
γ	ratio of specific heats for pulse-rocket exhaust gases, 1.22
ξ	fraction of critical damping for model pitching mode, b/ω
ξ_h	fraction of critical damping for wing bending mode, b_h/ω_h
ω	model pitching frequency, radians/sec
ω_h	wing bending frequency, radians/sec

MODEL AND TESTS

Model

The model used in this investigation consisted of a cylindrical fuselage with an ogival nose equipped with tapered wings unswept at the 50-percent-chord line. Vertical-tail fins provided yaw stability. A dimensioned sketch of the model is presented in figure 1 and photographs of the model are shown in figure 2. The asymmetrical fuselage bump shown in figures 1(b), 1(c), and 2(b) is an instrumentation fairing. The model dynamic constants were as follows:

Total weight, lb	82.5
Pitching moment of inertia, slug-ft^2	7.12
Yawing moment of inertia, slug-ft^2	7.24
Wing first bending frequency, cycles per second	93
Wing second bending frequency, cycles per second	157
Wing torsional frequency, cycles per second	359
Tail first bending frequency, cycles per second	70

The solid magnesuim-alloy wings had 5-percent-thick flat-plate sections with beveled leading and trailing edges. The wing had a taper ratio of 0.445, and aspect ratio of 3.45.

Twelve pulse rockets were mounted inside the fuselage. These rockets were manifolded in pairs (see fig. 2(c)). The rockets of each pair were fired simultaneously over each wing with a firing sequence as indicated in figure 1(b). Nozzles were positioned to exhaust in a spanwise direction about 1.2 inches above and below the wing chord plane. Figures 1(b) and 1(c) show pulse-rocket locations. Typical pulse-rocket performance data including a thrust-time curve are shown in figure 3. These data were determined previously for pulse rockets similar to those used in the present tests.

Flight Test

The flight test was conducted at the Langley Pilotless Aircraft Research Station at Wallops Island, Va. The model was boosted to a Mach number of 2.1 and then drag separated from the booster. During the coasting period which followed, data were telemetered to a ground receiving station and recorded.

Flight conditions resulted in the values of Reynolds number and dynamic pressure presented as a function of Mach number in figure 4.

INSTRUMENTATION

Inductance-type instruments measured time histories of model angle of attack, model normal and transverse acceleration, total pressure, and normal acceleration near the tips of both wing panels. Response of the measuring and recording instrumentation was such that no correction to the recorded data was required at the frequencies encountered in the tests.

A Rawin set AN/GMD-1A recorded atmospheric data at all flight altitudes. Flight-path data were obtained from tracking radar, and a CW Doppler velocimeter was used to determine flight velocity.

ACCURACY

The following information is included to indicate the possible error in the basic measurements. These values represent maximum error in evaluating isolated data. In computations involving differences (such as slope evaluations), possible errors in the individual quantities can be considered to be about one-half as large as those indicated except as noted otherwise (because zero-point uncertainty is about one-half the total error). When the quantities are used in the form of ratios (such as in the determination of damping decrements), the errors are estimated to be less than one-fourth the value indicated here.

Quantity	Error
Angle of attack, deg	
Maximum error	±0.70
Difference error	±0.10
Model normal acceleration, g units	±0.5
Model transverse acceleration, g units	±0.20
Left wing vibrometer, g units	±10
Right wing vibrometer, g units	±10

Error in Mach number is estimated to be less than 0.02. Errors in dynamic pressure are estimated to be less than ±5 percent.

RESULTS AND DISCUSSION

A sample portion of the telemeter record showing the response of the various instruments to a typical pulse-rocket disturbance is presented in figure 5.

Pulse-Rocket Effectiveness

One measure of the effectiveness of pulse rockets is the amount of force that they can produce. Figure 6 presents the measured pulse-rocket normal-force effectiveness (in coefficient form) as a function of Mach number. These values were obtained from the maximum incremental change in model normal acceleration which occurred before the model had any measurable angle-of-attack response. The data are not faired by a curve because each test point represents a different chordwise location of the pulse rockets as indicated by the figure. These loads occurred about 0.01 second after ignition of the pulse rockets in each case. Also included in figure 6 is a pulse-rocket thrust coefficient curve, which was obtained from figure 3 for an elapsed time from firing of about 0.01 second. The comparison of this curve with the test points shows that the loads developed on the wing were from about 5 to 8 times as large as the thrust of the pulse rockets (at the time $|\Delta C_N|$ was obtained). Because these data contain the combined effects of both Mach number and pulse-rocket location along the chord, and since small variations in the ignition times of the manifolded rockets can have some effect on the initial loads produced, no other results were concluded.

Another indication of the pulse-rocket effectiveness is the maximum incremental response from trim in model angle of attack. This information is presented in figure 7(a) as a function of Mach number. Again, no curve has been faired through the data because the data points represent different chordwise locations of the pulse rockets. As would be expected, the increased model stability at the higher Mach numbers reduces the general level of the test points. Shown for comparison in figure 7(a) are calculated values of the peak angle-of-attack response for the test pulse rockets mounted vertically (without the interference effects of the wing) at the same longitudinal fuselage locations. The comparison shows that exhausting the pulse rockets over the wing results in larger angles of attack than were calculated for the interference-free normal pulses. The ratio of measured peak α response to the peak α response calculated for vertical pulse rockets is shown in figure 7(b). This ratio was found to correlate better with chordwise location of the pulse rockets than with Mach number and ranged from about 2 to 5 with the larger ratios being obtained by pulse rockets located nearer the wing

leading edge. It should be noted, however, that the vertical pulse rockets could be located farther from the model center of gravity to provide increased response whereas those exhausting over the wing are restricted in this sense.

It should be mentioned that the pulse rockets used in this investigation were not particularly well adapted to the purpose of obtaining a large α response with the model used.

Wing Damping

Wing-damping data were obtained from the logarithmic rate of decay of the wing bending oscillations which were excited by the pulse rocket exhausts. Figure 8 shows the amplitude response of both wing-tip vibrometers to the excitations of pulse rocket number 1. These oscillations are shown in figure 5. A power spectrum, obtained for all such vibrometer oscillations, indicated that although higher modes (principally second bending) were excited by the pulse rockets, the energy absorbed at these higher frequencies was small, and the measured wing response was essentially in the first bending mode. Values of wing damping were the same for both wing panels and are presented in figure 9 as a fraction of critical damping at the various Mach numbers. The structural or tare damping of the first bending mode was measured previous to the flight test and is shown to be about 2 percent of critical. The difference between the test points and the tare damping level (in fig. 9) then represents the amount of aerodynamic damping in the first bending mode. Values of reduced frequency of the wing associated with these damping data ranged from 0.17 to 0.29 and are presented in figure 10 as a function of Mach number.

With regard to gathering wing damping data at the higher wing modes, it is evident that a more abrupt input disturbance would be necessary to excite these modes. Also, the location of the acceleration pickups on the wing could be adapted to amplify individual modes.

It is concluded, therefore, that pulse rockets arranged to induce loads on adjacent wings offer a simple and effective means of exciting wing oscillations for flight flutter purposes without affecting the wing response.

Model Stability Data

Values of C_{m_α}, C_{N_α}, and model pitch damping are presented in figures 11, 12, and 13, respectively, as a function of Mach number.

These curves are typical and are included without discussion as a matter of interest.

CONCLUDING REMARKS

Exhausting small pulse rockets spanwise across a wing in free flight at Mach numbers from 0.9 to 1.8 induced normal-force loads from 5 to 8 times as large as the corresponding thrust of the pulse rockets.

The maximum angles of attack produced by the pulse-rocket disturbances was from 2 to 5 times as large as the peak angles of attack calculated for vertically mounted pulse rockets at the same longitudinal stations (with wing-interference effects neglected). For the firing sequence used, which involved a wide variation in flight Mach number, the increase in effectiveness in producing peak angle of attack was greater for pulse rockets located nearer the wing leading edge.

The pulse rockets used offer a simple and effective means of exciting wing oscillations for flight flutter-testing purposes without affecting the wing response.

Langley Aeronautical Laboratory,
National Advisory Committee for Aeronautics,
Langley Field, Va., July 16, 1958.

REFERENCES

1. Arbic, Richard G.: Free-Flight Investigation at Transonic Speeds of the Stability Characteristics of a Tailless Missile Configuration having a 45° Sweptback Wing of Aspect Ratio 4. NACA RM L56E11, 1956.

2. Falanga, Ralph A., and Janos, Joseph J.: Pressure Loads Produced on a Flat-Plate Wing by Rocket Jets Exhausting in a Spanwise Direction Below the Wing and Perpendicular to a Free-Stream Flow of Mach Number 2.0. NACA RM L58D09, 1958.

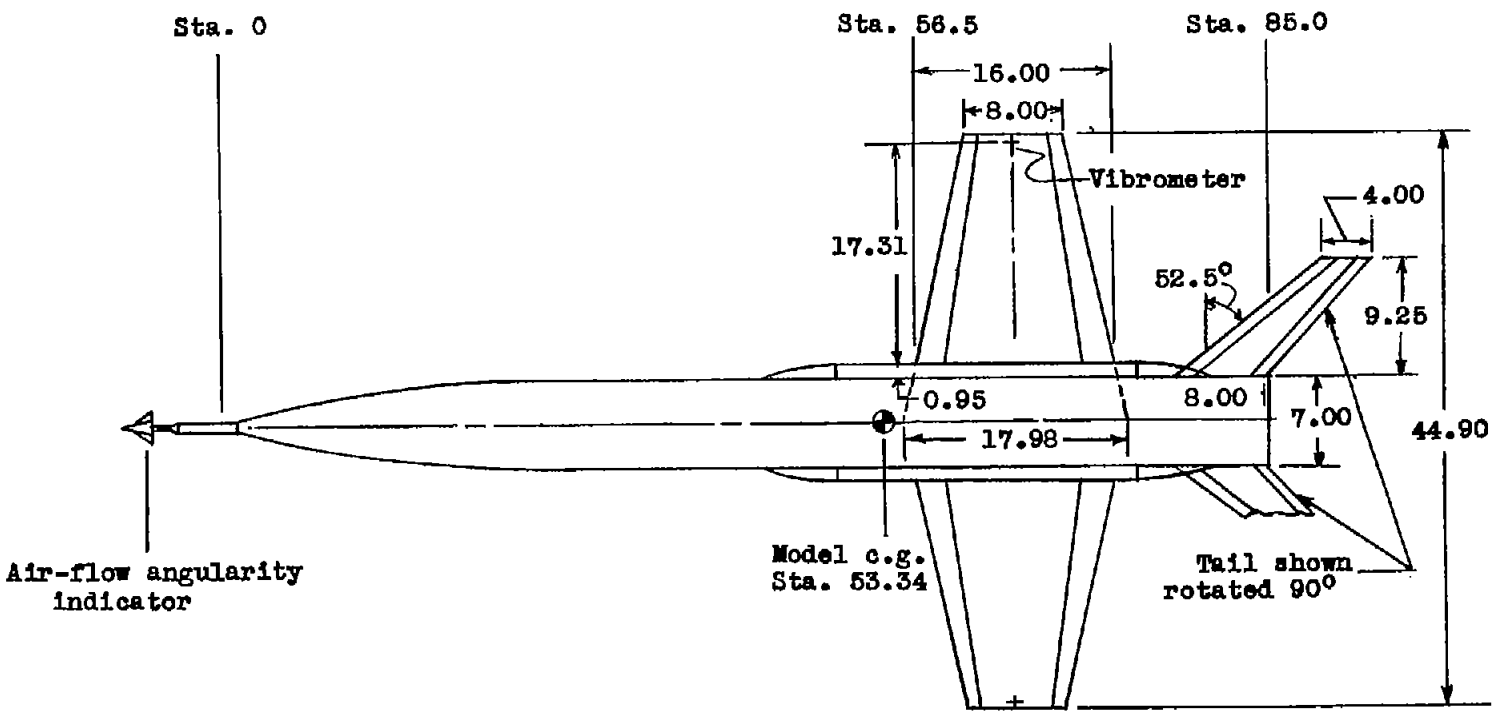

(a) Plan view.

Figure 1.- Model design. All dimensions in inches.

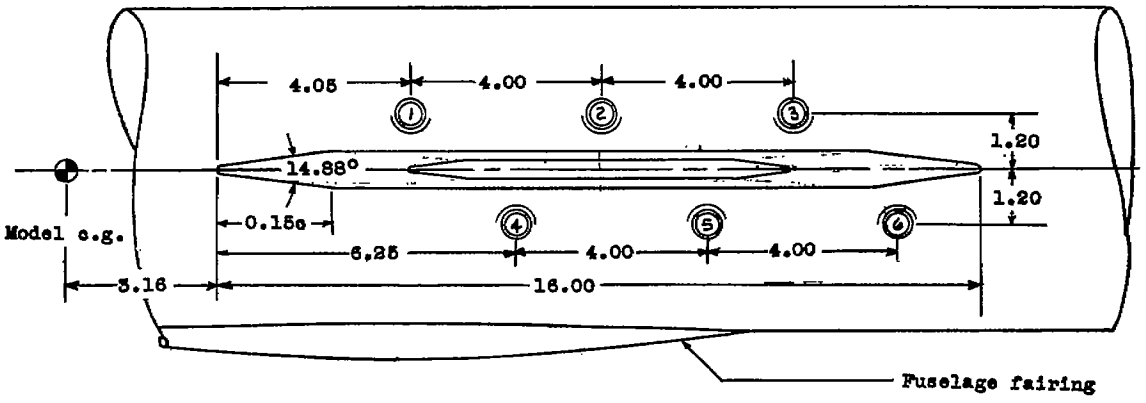

(b) Side view showing pulse-rocket-nozzle locations. Firing sequence indicated by nozzle numbers.

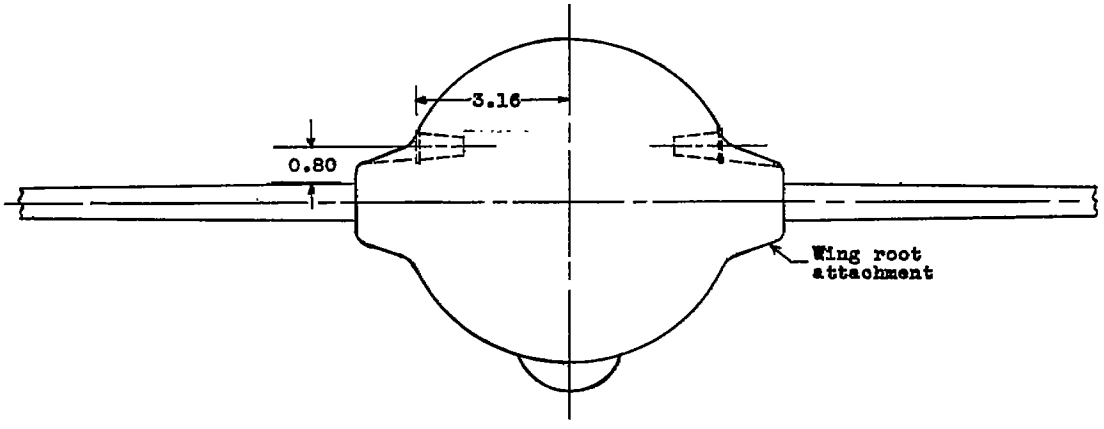

(c) End view showing typical pulse-rocket-nozzle locations.

Figure 1.- Concluded.

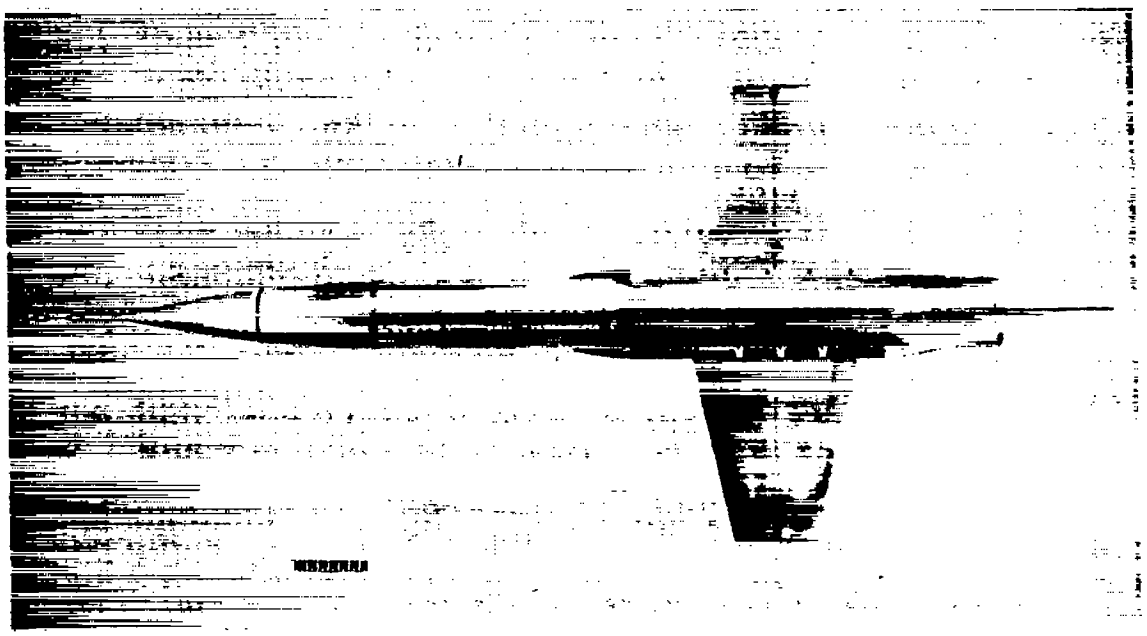

(a) Top plan view.

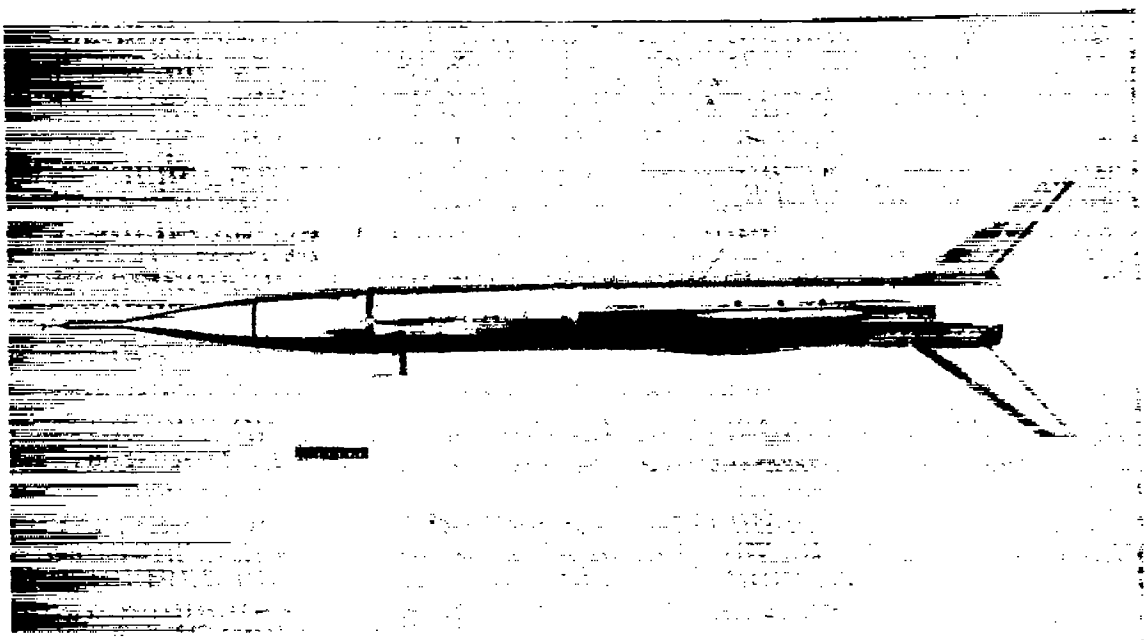

(b) Left side view. L-58-2516

Figure 2.- Test vehicle.

[redacted]

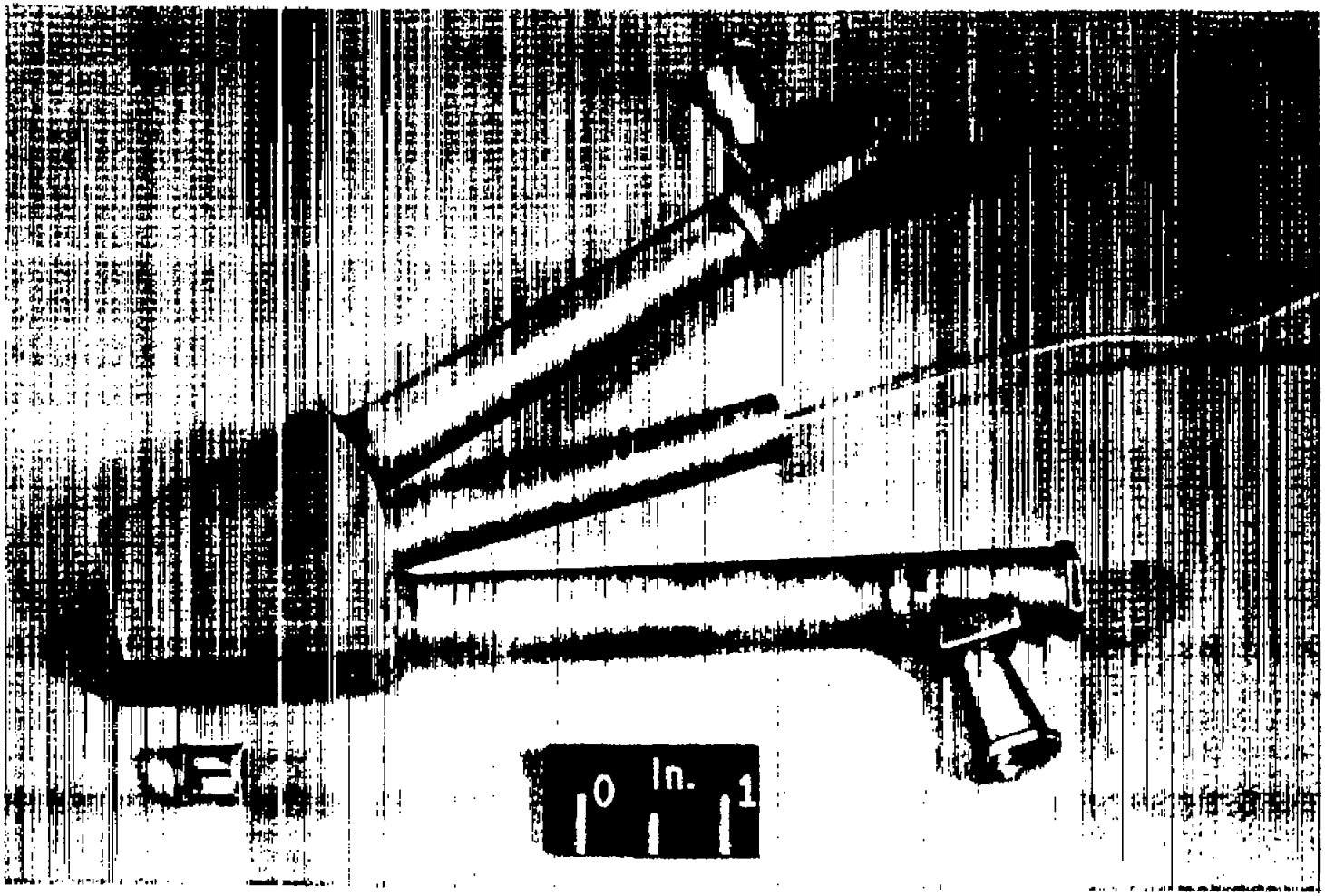

(c) Pulse-rocket unit. L-57-3294

Figure 2.- Concluded.

[redacted]

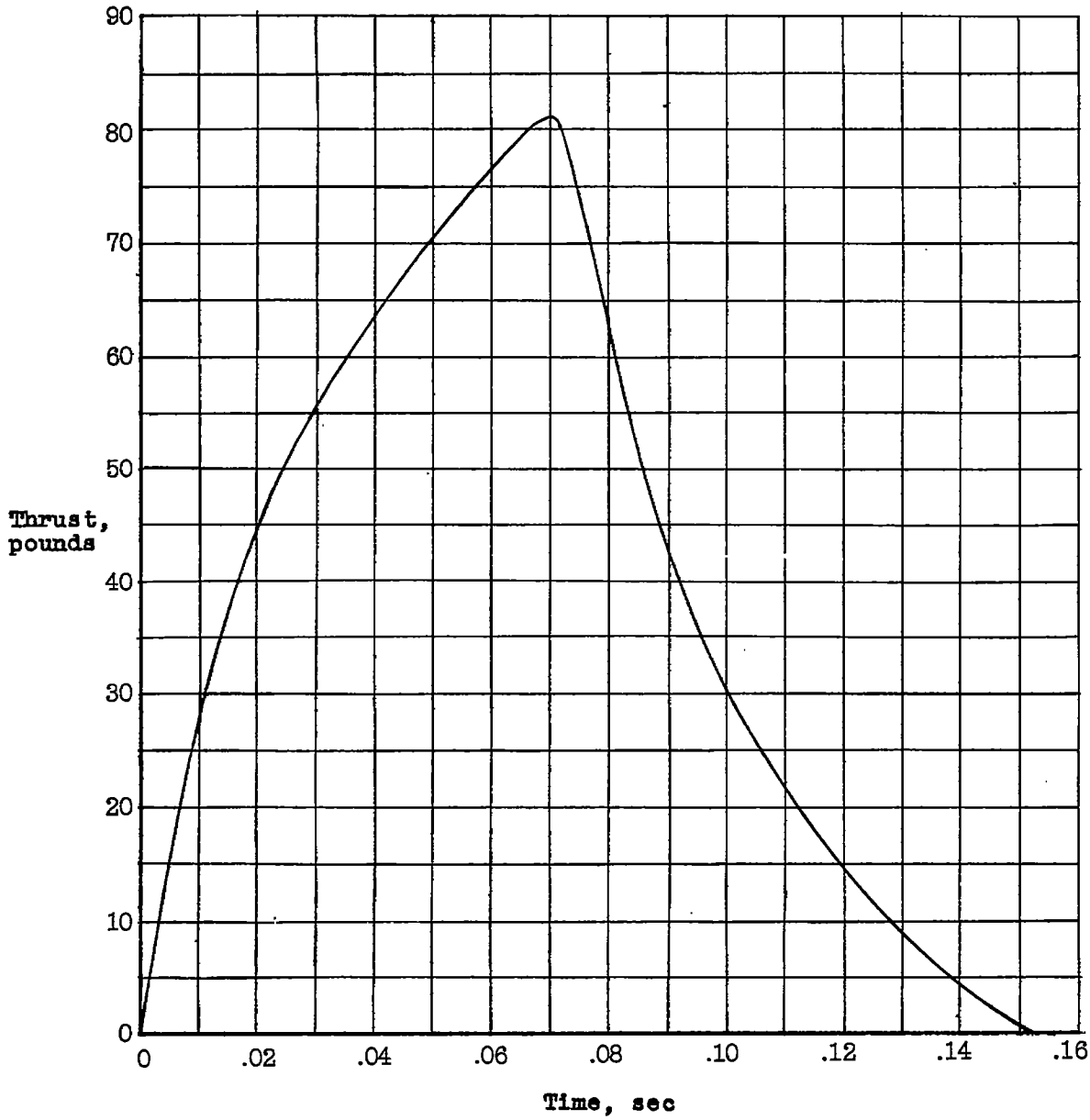

Figure 3.- Pulse-rocket performance characteristics. Typical for 60° F. Total impulse, 6.04 lb-sec. Exit Mach number = 3.143; γ = 1.22; propellant weight = 0.027 lb.

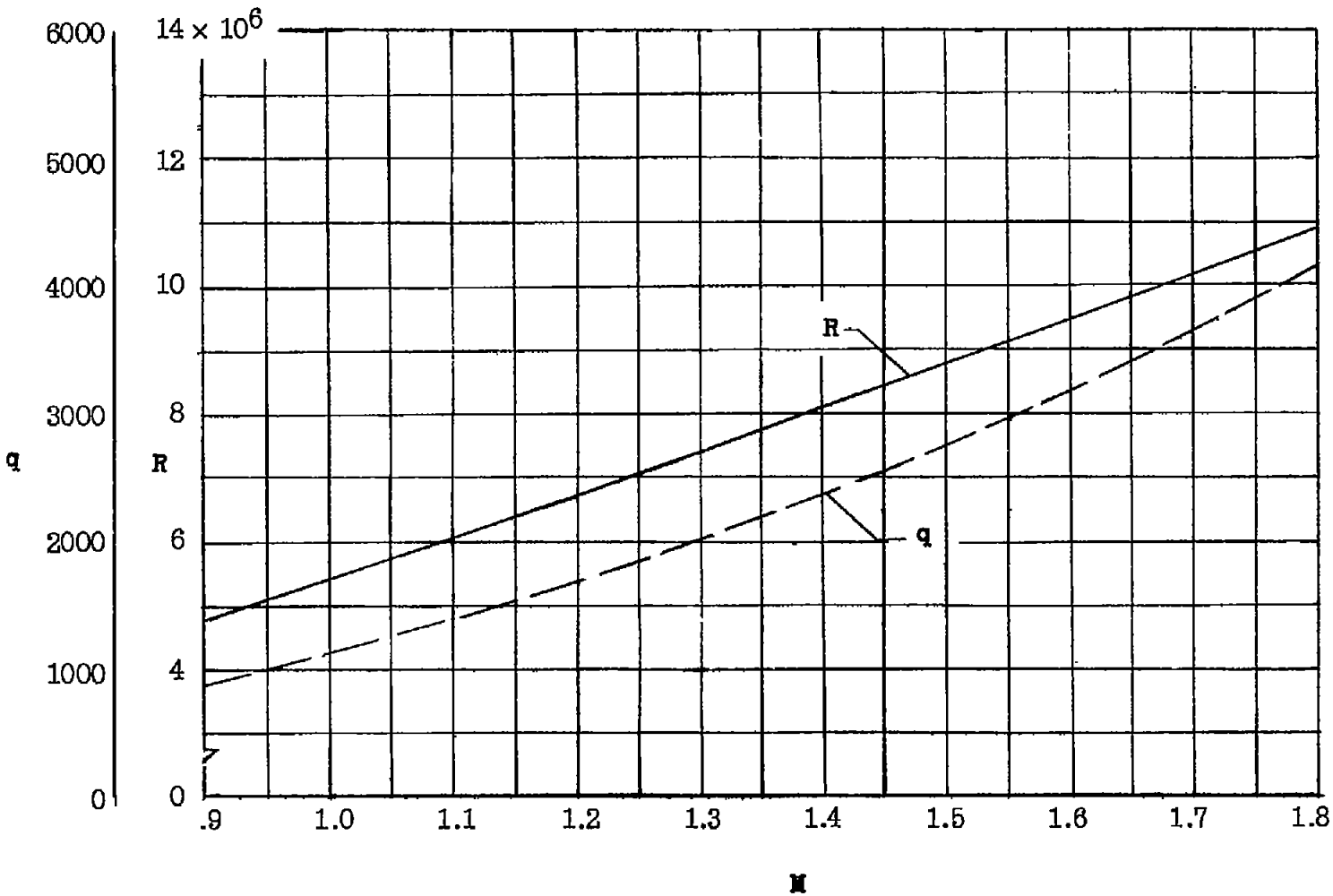

Figure 4.- Variation of Reynolds number and dynamic pressure with Mach number.

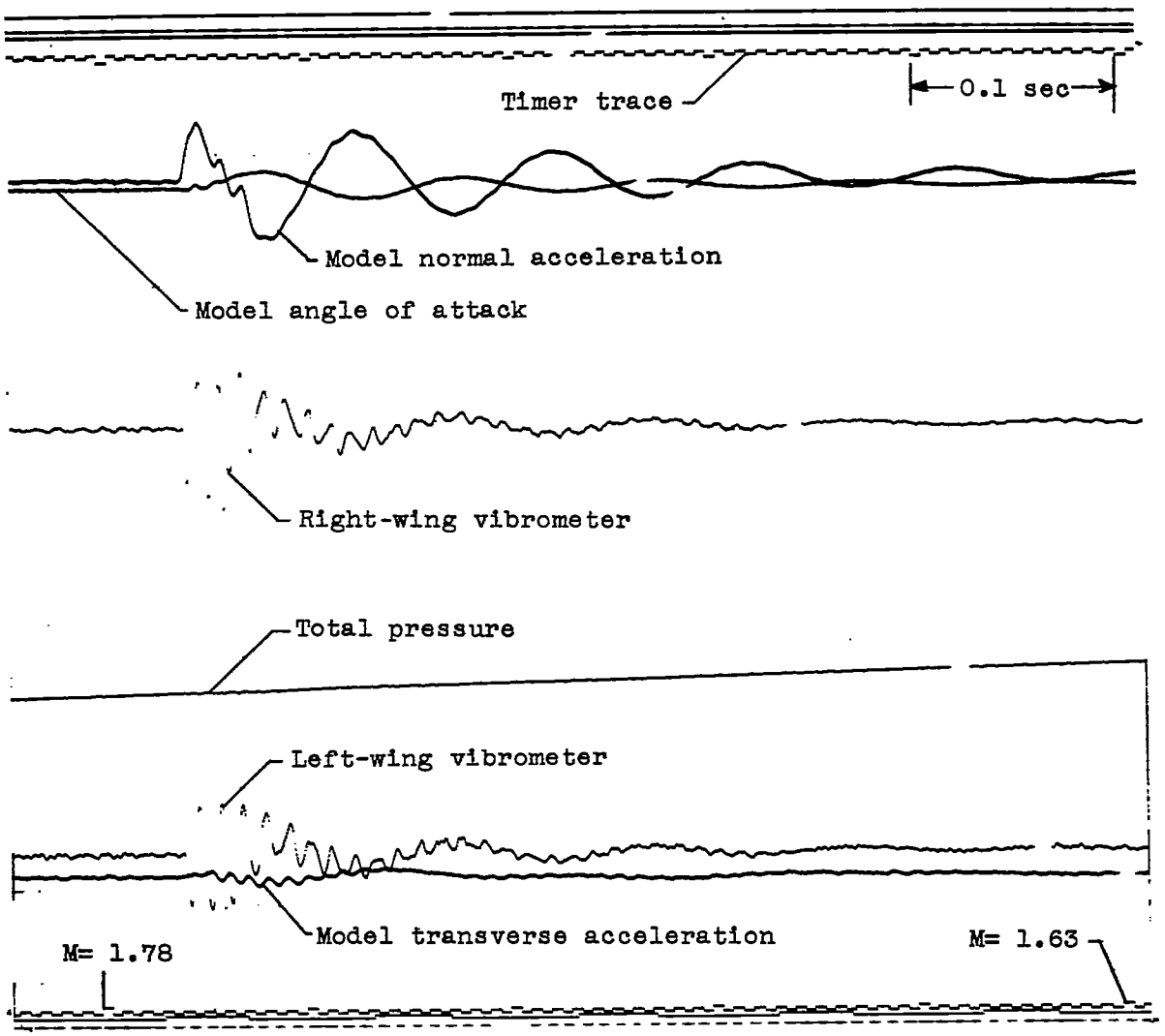

Figure 5.- Sample section of telemeter record. Pulse number 1.

[redacted]

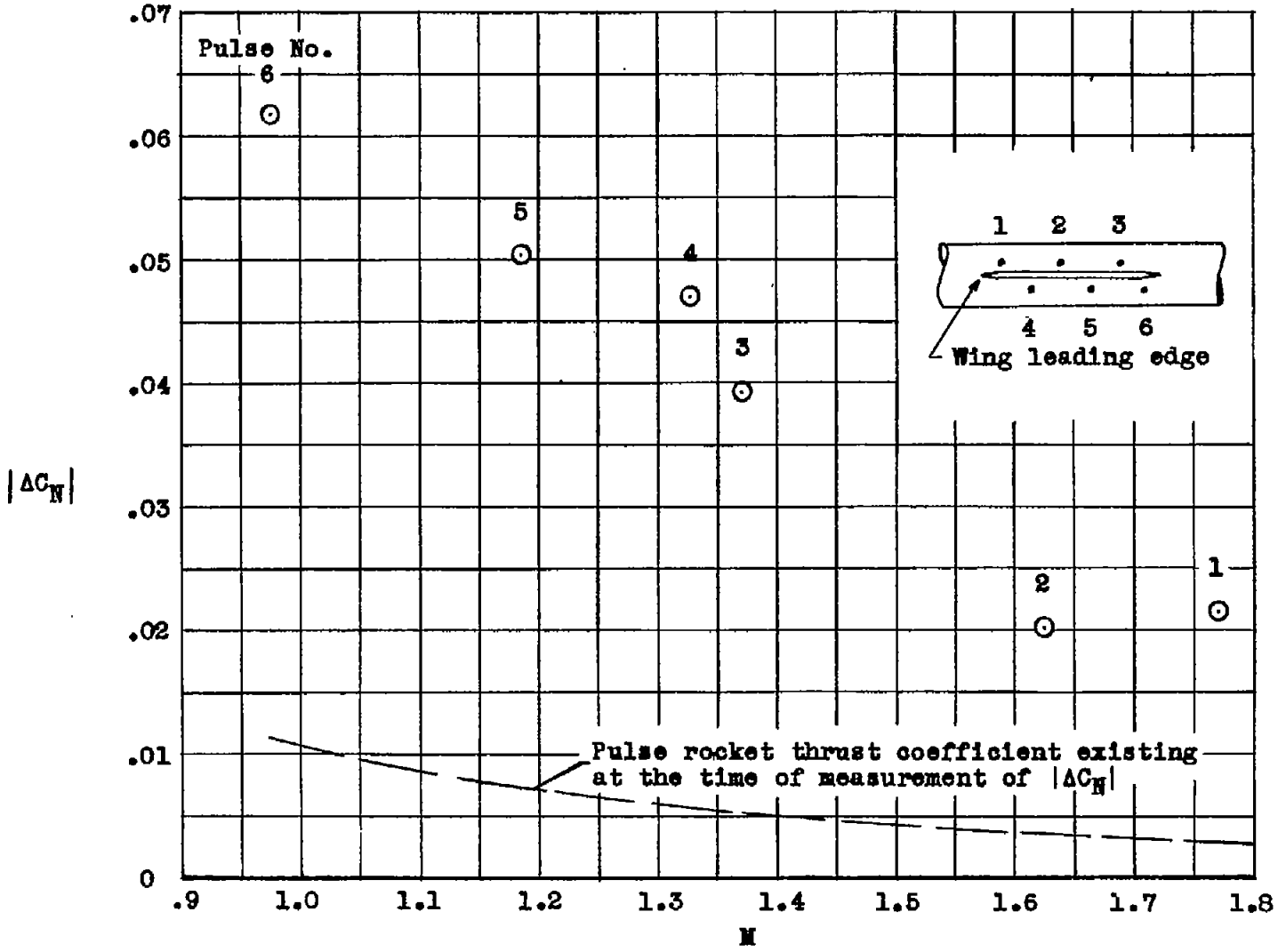

Figure 6.- Pulse-rocket normal-force effectiveness as a function of Mach number. Pulse-rocket thrust coefficient also shown. Firing sequence indicated by pulse number.

[redacted]

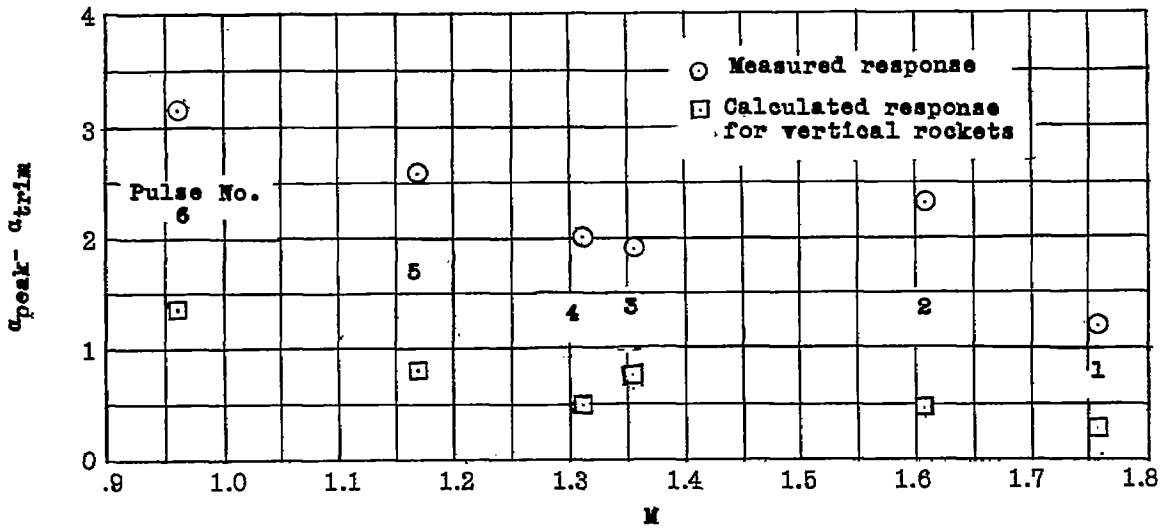

(a) Variation of peak α response with Mach number.

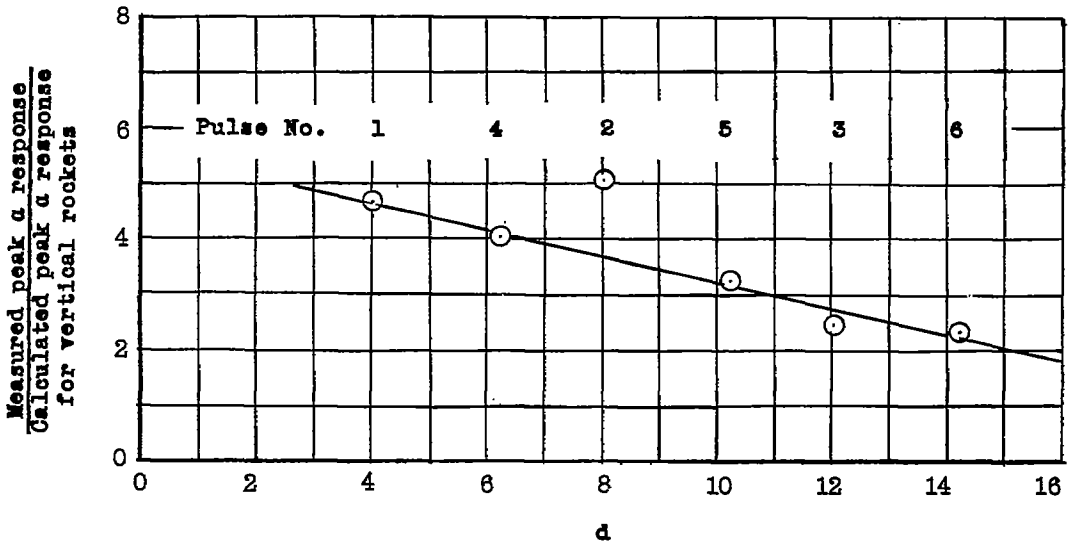

(b) Ratio of measured peak α response to calculated peak α response for vertical rockets as a function of rocket location along the wing chord.

Figure 7.- Effectiveness of pulse rockets as angle-of-attack producers. Firing sequence indicated by pulse number.

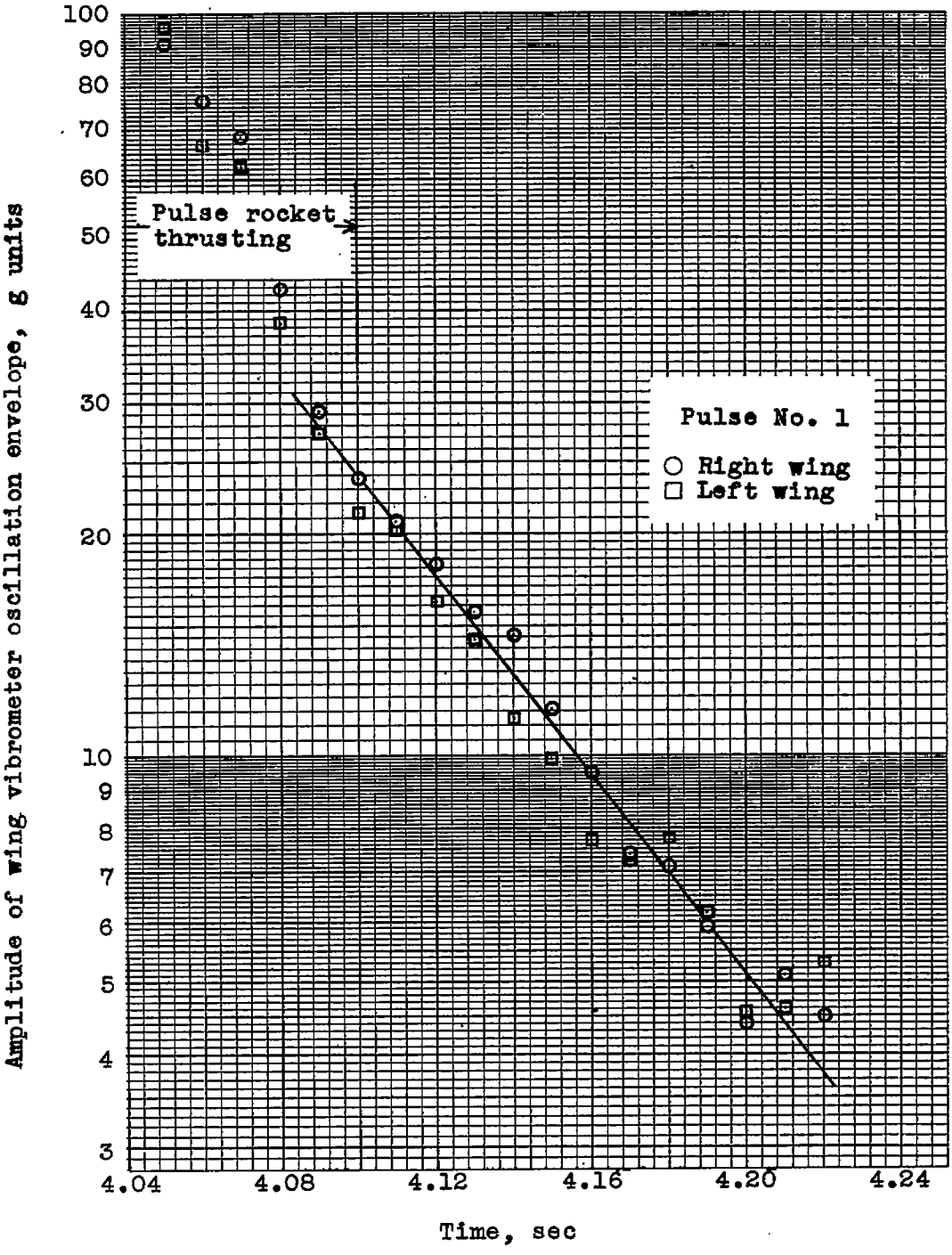

Figure 8.- Typical time history of wing vibrometer envelopes for pulse number 1.

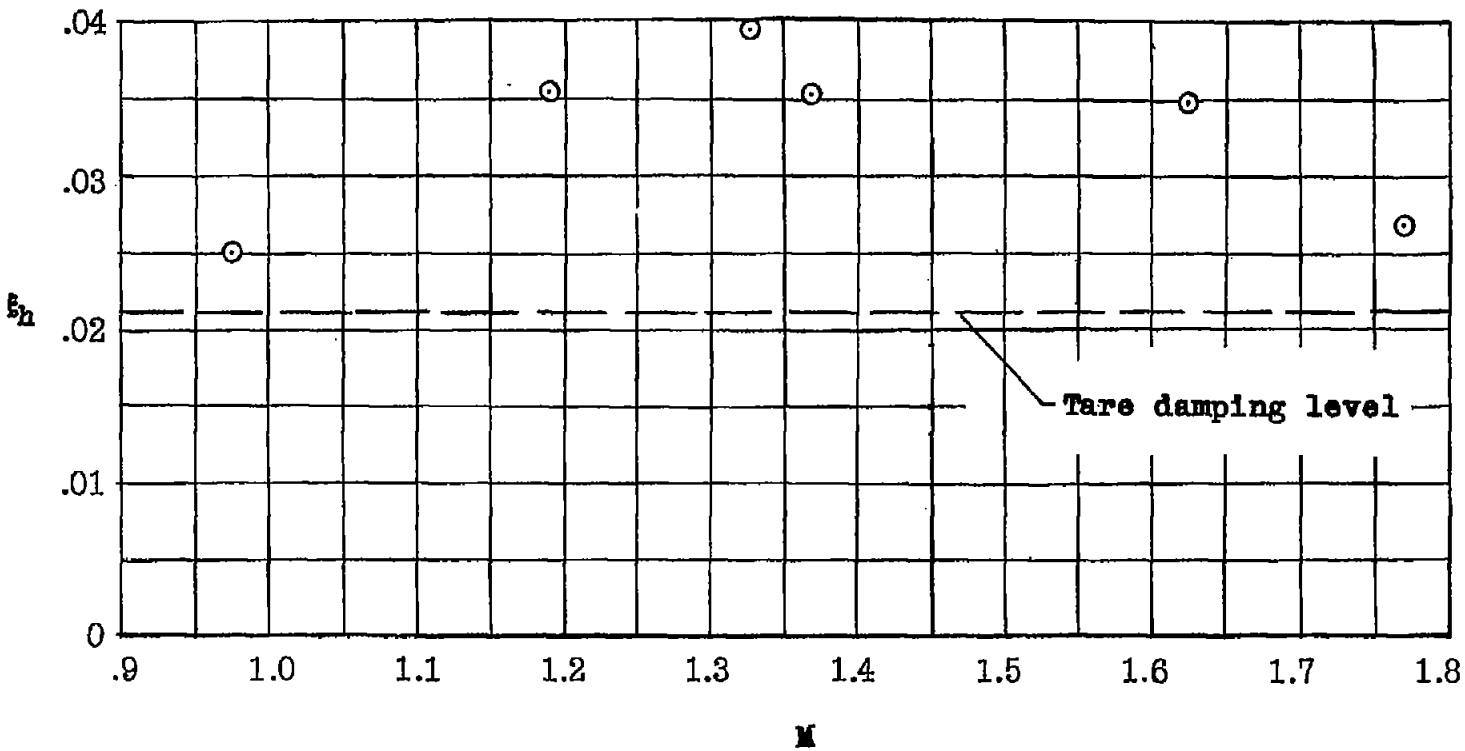

Figure 9.- Wing damping (first bending mode) as a function of Mach number.

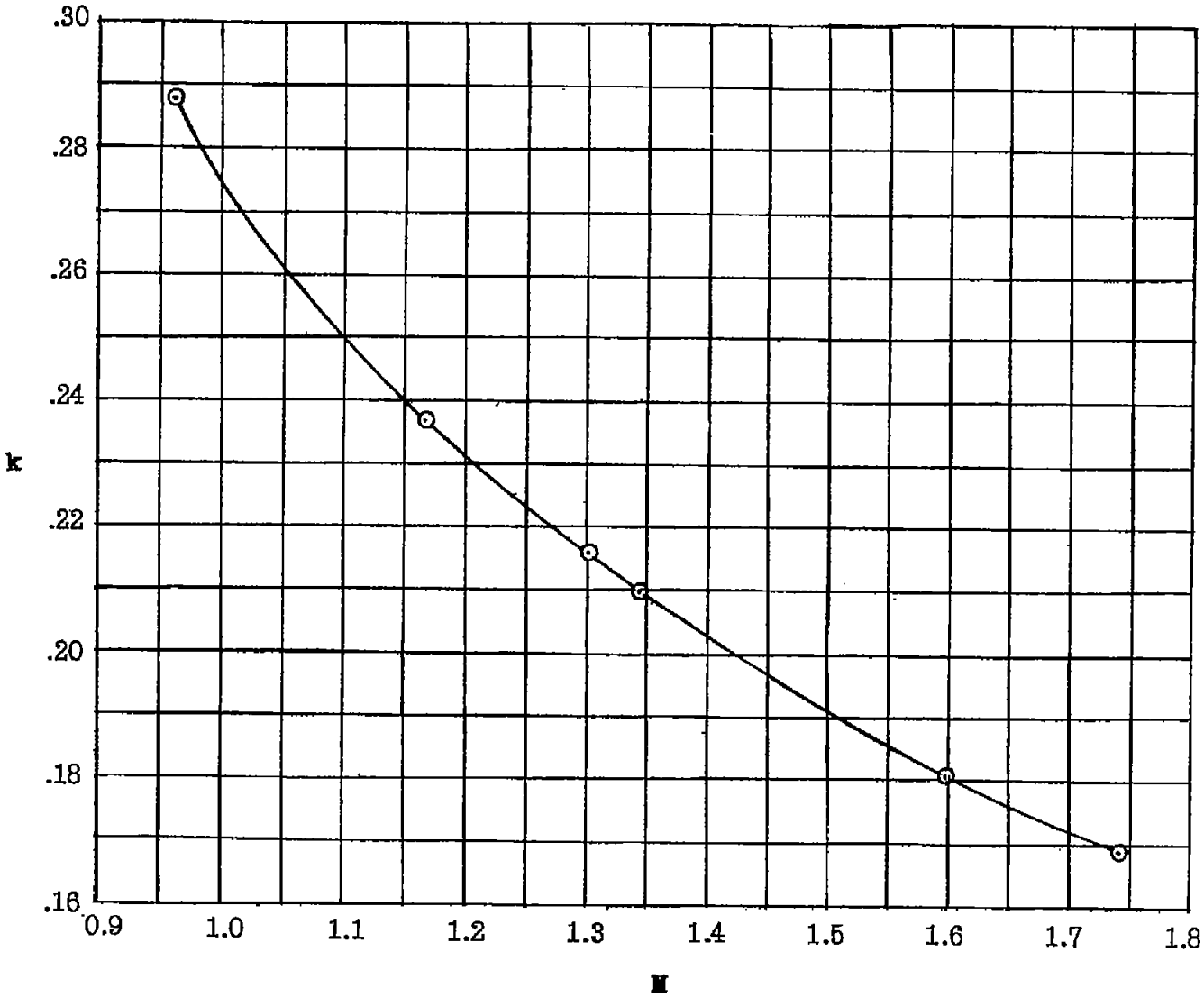

Figure 10.- Variation of wing reduced frequency with Mach number.

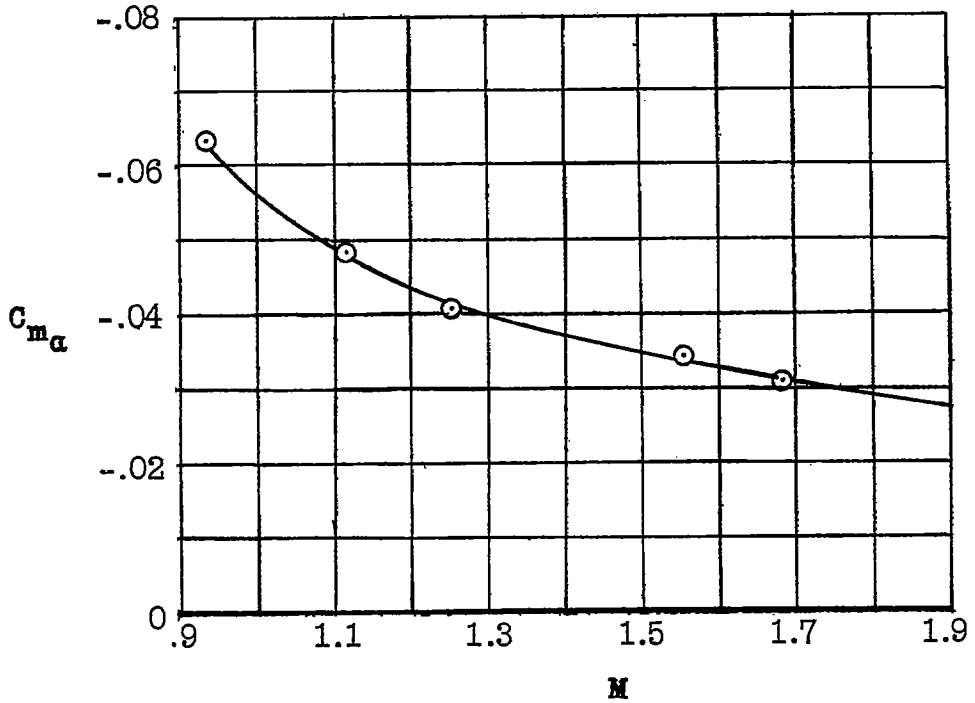

Figure 11.- Static stability derivative C_{m_α} as a function of Mach number.

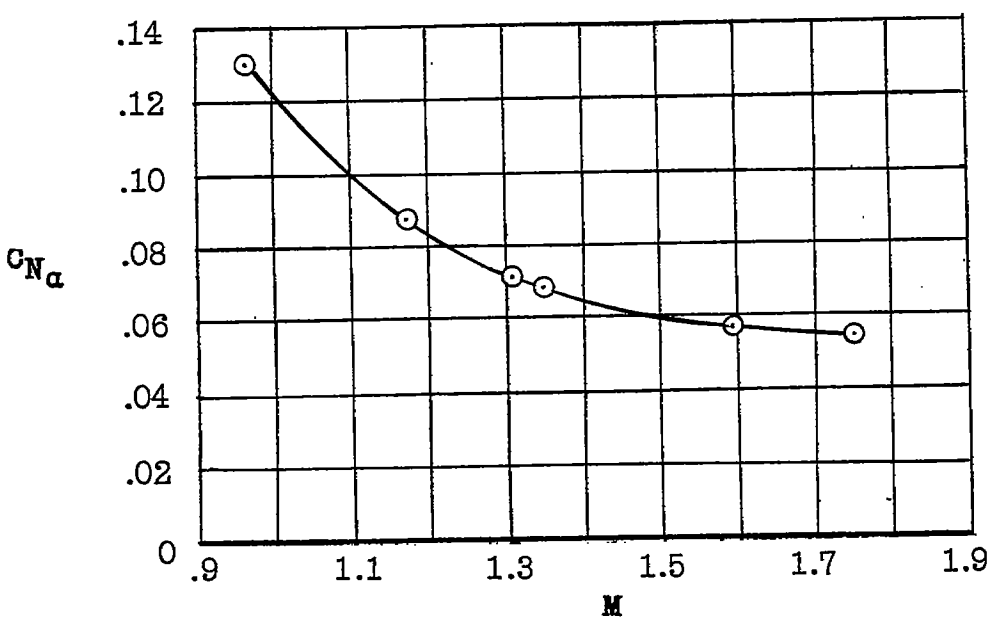

Figure 12.- Effect of Mach number on model normal-force effectiveness.

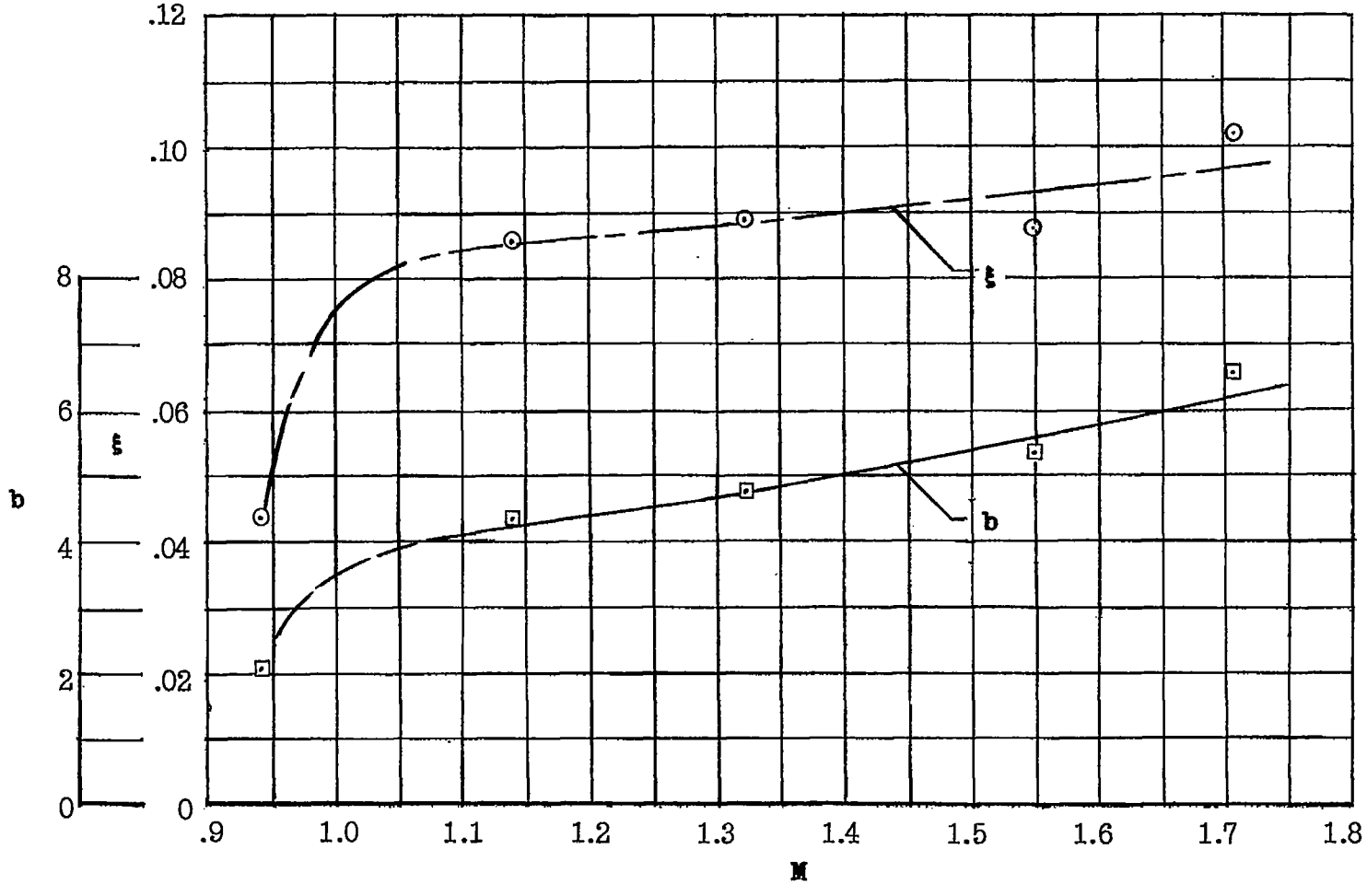

Figure 13.- Effect of Mach number on model pitch damping.